THE JOURNAL OF COMPARATIVE NEUROLOGY 373:139–155 (1996)

Mitochondrial- and Nuclear-Encoded Subunits of Cytochrome Oxidase in Neurons: Differences in Compartmental Distribution, Correlation With Enzyme Activity, and Regulation by Neuronal Activity

FENG NIE AND MARGARET T.T. WONG-RILEY
Department of Cellular Biology and Anatomy, Medical College of Wisconsin, Milwaukee, Wisconsin 53226

ABSTRACT

Cytochrome oxidase (CO), a mitochondrial energy-generating enzyme, contains both mitochondrial- and nuclear-encoded subunits. In neurons, local levels of CO activity vary among different neuronal compartments, reflecting local demands for energy. The goals of the present study were to determine if compartmental distribution of CO subunit proteins from the two genomes was correlated with local CO activity, and if their expression was regulated proportionately in neurons. The subcellular distributions of mitochondrial-encoded CO III and nuclear-encoded CO Vb proteins were quantitatively analyzed in mouse cerebellar sections subjected to postembedding immunocytochemistry. Local levels of subunit proteins were also compared to local CO activity, as revealed by CO cytochemistry. In order to study the regulation of subunit protein expression, we assessed changes in immunoreactivity of the two CO subunits as well as changes in CO activity in mouse superior colliculus after 1 to 7 days of monocular enucleation. We found that immunoreaction product for both CO III and CO Vb existed almost exclusively in mitochondria, but their compartmental distributions were different. CO III was nonhomogeneously distributed among different neuronal compartments, where its local level was positively correlated with that of CO activity. In contrast, the subcellular distribution of CO Vb was relatively uniform and did not bear a direct relationship with that of CO activity. Moreover, the two subunit proteins were disproportionately regulated by neuronal activity. CO III and CO activity exhibited parallel decreases after the deprivation of afferent input, and their changes were earlier and to a greater degree than that of CO Vb proteins. Thus, the present findings indicate that the local expression and/or distribution of CO subunit proteins from the two genomes may involve different regulatory mechanisms in neurons. Our data also suggest that the activity-dependent regulation of mitochondrial-encoded CO subunits is likely to play a major role in controlling the local levels of CO content and its activity.

Indexing terms: mitochondria, oxidative metabolism, ultrastructure, immunocytochemistry, central nervous system

Neural functional activity is an energy-requiring process, and it, in turn, dynamically regulates energy production in neurons (Krnjevic, 1975; Mata et al., 1980). Since the brain derives nearly all of its energy from oxidative metabolism, the content and/or activity of energy generating enzymes in mitochondria should faithfully reflect the normal level of energy demand of a cell or its compartments (Erecinska and Silver, 1989; Wong-Riley, 1989, 1994). Cytochrome oxidase (CO), a terminal complex of the mitochondrial respiratory chain, catalyzes the transfer of electrons from cytochrome c to molecular oxygen, generating ATP via the coupled process of oxidative phosphorylation (Wikstrom et al., 1981; Kadenbach et al., 1987). Mitochondria in different

Accepted May 3, 1996.

Address reprint requests to Dr. Margaret T.T. Wong-Riley, Department of Cellular Biology and Anatomy, Medical College of Wisconsin, 8701 Watertown Plank Road, Milwaukee, WI 53226.

neurons, neuronal processes, and even compartments of the same neuron do possess different levels of CO activity (shown cytochemically), which are positively correlated with local levels of physiological activity (reviewed by Wong-Riley, 1989, 1994). It is still not known, however, whether the local level of CO activity in neuronal compartments is dependent mainly upon the local amount of CO proteins.

Cytochrome oxidase in mammalian cells comprises 13 subunits, the first three of which are mitochondrial-encoded and the rest are nuclear-encoded (Kadenbach et al., 1983; Azzi and Muller, 1990; Capaldi, 1990). The biosynthesis of CO holoenzyme requires the coordination of mitochondrial- and nuclear-encoded subunits (Poyton et al., 1988; Azzi and Muller, 1990; Capaldi, 1990). The nuclear-encoded CO mRNAs in neurons were found exclusively in neuronal somata, while mitochondrial-encoded CO mRNAs were distributed throughout the cell bodies and neuronal processes (Hevner and Wong-Riley, 1991, 1993; Wong-Riley et al., 1994). Thus, the separation of the two genomes requires the existence of a mechanism that posttranslationally regulates the distribution of CO subunit proteins from two genomic sources for the assembly of CO holoenzyme. The precursor proteins of nuclear-encoded CO subunit IV are delivered within the mitochondria from the somata to distal neuronal processes, where they form a precursor pool for the assembly of CO holoenzyme (Liu and Wong-Riley, 1994). It is not known if CO subunit proteins from the two genomes are proportionately distributed among various neuronal compartments, and if their levels are correlated with the local level of CO activity. Verification of this issue requires quantitative EM analysis in CO immuno-reacted tissue. Previously, we found that the expressions of mitochondrial and nuclear genes for CO are not coordinately regulated by neuronal activity (Hevner and Wong-Riley, 1993). Decreases in mitochondrial- and nuclear-encoded mRNA levels were disproportionate in lateral geniculate nucleus (LGN) of the monkey after retinal impulse blockade, suggesting that the expression of CO subunit mRNAs from the two genomes involves different regulatory mechanisms. This poses an important question as to whether their gene products, CO subunit proteins, are also differentially regulated.

The purposes of the present study were to examine the subcellular distributions of mitochondrial- and nuclear-encoded CO subunit proteins in normal neurons, to determine if their distribution bears any relationship with local CO activity, and to compare the time course and degree of their changes after the removal of sensory input. To differentiate between CO subunit proteins from the two genomes at the subcellular level, two antibodies, one against CO subunit III (mitochondrial-encoded) and one against CO Vb (nuclear-encoded), were generated and used to label CO by postembedding immunogold technique at the EM level. The rodent cerebellum was used as a model, because its ultrastructural features and subcellular distribution of CO activity (shown cytochemically) have been well characterized (Palay and Chan-Palay, 1974; Mjaatvedt and Wong-Riley, 1988). Subcellular distributions of immunoreactivity for the two subunits in the cerebellum were quantitatively analyzed, and their local levels were compared to local CO activity, as revealed by CO cytochemistry. In order to study the regulation of the two CO subunits, we used the mouse superior colliculus as a model, and quantitatively compared changes in the relative amount of each CO subunit proteins as well as in the relative level of CO activity 1 to 7 days after monocular enucleation.

MATERIALS AND METHODS

Peptide synthesis and antibody production

Based on the peptide sequence program of GCG Database, two sequences from different CO subunits of murine genomes were chosen for synthesis as antigens. One was a sequence of 15 amino acids from residues 59–74 of CO III encoded by the mitochondrial genome of mouse L cell: RDVIREGTYQGHHTP (Bibb et al., 1981). The other was comprised of 14 amino acids from residues 107–120 of CO Vb, encoded by the nuclear genome of mouse skeletal muscle: KGESQRCPNCGTHY (Basu and Avadhani, 1991). Recently, our analysis of DNA sequences from murine brain CO has confirmed that the above two sequences were identical with the corresponding sequences derived from the brain (Wong-Riley et al., 1994). In addition, peptide-structure prediction from GCG indicated that both sequences have a high antigenic potential based on their surface probability, hydrophilicity, and antigenic indices. They are also highly homologous to corresponding CO subunits from human (86.6% identity for CO III and 76% for CO Vb), but bear little homology with any other known protein sequences, including those of the other CO subunits. These two polypeptides were then synthesized by a MilliGen 9050 peptide synthesizer by using the solid-phase method, and reached an approximate 100% purity without high-performance liquid chromatography (HPLC) purification.

The synthetic peptides were coupled to the carrier protein keyhole limpet hemocyanin (KLH) with a glutaraldehyde link. The following procedures (Harlow and Lane, 1988) were used for the coupling of each synthetic peptide: (1) KLH (10 mg) was dissolved in 2 ml of 0.1 M borate buffer (pH 10) and mixed well with 10 mg of synthetic peptide; (2) cross-linking was carried out by the addition of 1 ml of 0.3% glutaraldehyde (1° grade), and the mixture was incubated at room temperature (RT) for 2 hours until the solution turned yellow; (3) unreacted glutaraldehyde was blocked by 0.25 ml of 1 M glycine for 30 minutes at RT; and (4) excess free peptide and glutaraldehyde were removed by dialysis in 3 liters of 0.1 M borate buffer (pH 8.5), with several changes overnight at 4°C.

Two female New Zealand White rabbits were immunized with each peptide-protein conjugate (CO III or CO Vb). Each animal received initial injections of 0.5 ml of the peptide-glutaraldehyde-KLH conjugate (1.0 mg) and an equal volume of complete Freund's adjuvant, at about 40 intradermal sites on its back. After 8 weeks, boosters of 1 mg of conjugate emulsified with an equal amount of incomplete Freund's adjuvant were given to each animal.

IgG's purification

Affinity columns were made by coupling each synthetic subunit peptide to Affi-gel 10 through activated ester bonds. Immunoglobins (IgGs) against each subunit sequence were purified by passing antisera over the affinity column followed by washes with 40 mM HEPES. The column was then eluted with 0.1 M glycine, pH 2.8. Purified IgGs were neutralized with 1 M Tris buffer, pH 10. The concentration of purified IgG solutions was determined spectrophotometrically at 280 nm, using an extinction coefficient of 1.4. IgGs rather than antisera against differ-

ent CO subunits were always used for CO immunocytochemstry due to their low background staining.

Enzyme-linked immunosorbent assay (ELISA)

The two antibodies against different CO subunits were creened with their corresponding synthetic peptide by neans of ELISA. The antibody titers, defined as the naximal dilution of an antibody in which immunoreaction roduct can be detected, were also determined by this assay. olystyrene flat-bottom wells were coated with 100 μl of eptide-carrier protein conjugates (containing 1 μg of peptide and 1 μg of KLH) in 0.1 M $NaHCO_3$, pH 9.0, and ncubated overnight at 4°C. After coating with peptide-rotein conjugate, the wells were blocked for 2 hours with % normal goat serum (NGS). Primary and secondary ntibodies (goat anti rabbit IgG-HRP) were diluted with 5% IGS in PBS buffer and reacted at RT for 2 hours, respecively. Color was developed with 2,2′-azinobis (3-ethylbenothiazoline-6-sulfonic acid). The reaction was stopped by he addition of 25 μl/well 10% SDS. The A_{650} nm value in ach well was read on a Bio-Tek EL 309 Microplate utoreader. The following controls were used for antibody creening: (1) Each type of IgG was preadsorbed with its ynthetic peptide; (2) preimmune sera; (3) KLH only; (4) ytochrome P_{450} synthetic peptide; (5) KLH linked to P_{450} ia glutaraldehyde; and (6) glutaraldehyde.

Gel electrophoresis

Urea-sodium dodecylsulfate-polyacrylamide gel electrohoresis (SDS-PAGE) was performed according to the rocedure of Kadenbach et al. (1983) and by using a Bio-Rad Protean II apparatus and 1.5 mm thick gels. ortical gray matter of adult mouse brain was solubilized in 0% (wt/vol) SDS, at a ratio of 1 mg tissue/5 μl 10% SDS. omogenized tissue samples were run on urea-SDS-15% olyacrylamide gel for immunoblotting. Molecular weight tandards and purified CO holoenzyme from bovine brain ere also run in the same gel and silver-stained as described y Hevner and Wong-Riley (1989).

Immunoblotting

Proteins were transferred electrophoretically from polycrylamide gels to nitrocellulose by the procedure of Towin et al. (1979) as modified by Hevner and Wong-Riley 1989). For immunolabeling, blots were blocked with 5% on-fat dry milk (NFDM) in PBS overnight at 4°C. The lots were incubated overnight at 4°C with primary antibodes (anti-CO III, 1:2,000 or anti-CO Vb, 1:2,000) or preimune sera (1:2,000), washed, then incubated with secondry antibodies (GaR-HRP, 1:2,000) for 4 hours at RT. The lots were finally washed in phosphate buffered saline PBS) containing 0.2% Tween 20 and developed for 10 inutes at RT with 0.01 mg/ml 4-chloro-naphthol and .01% H_2O_2 in 1:5 of methanol:PBS.

Animal tissue preparation

Ten adult mice (BALB/c) were used in the study of ormal animals at the light microscopic level. The mice ere deeply anesthetized with an intraperitoneal injection f sodium pentobarbital (35 mg/kg body weight). The nimals were perfused via the left ventricle with 40 ml of .9% warm saline (37°C) followed by 50 ml of fixative (4% araformaldehyde in 4% sucrose, 0.1 M PBS, pH 7.6) at RT. rain tissues were cryoprotected in 10%, 20%, and 30% ucrose in 0.1 M PBS. The cerebella were frozen-sectioned coronally at 20 μm thickness. Alternate serial sections were processed for (1) CO histochemistry, (2) immunohistochemistry with antibody against CO subunit III, (3) immunohistochemistry with CO subunit Vb antibody, and (4) the controls with either preimmune sera or IgGs preadsorbed with the corresponding synthetic peptides. Twenty-four adult mice were used to study the regulation of CO subunits and CO activity in the superior colliculus. Right eyes of these animals were removed by surgical excision under anesthesia and the animals survived from 1 to 7 days (three mice were used for each single day, including the normal control). Adjacent sections of the superior colliculus were processed for CO histochemistry and CO immunohistochemistry with anti-CO III and CO Vb, respectively, as mentioned earlier. For EM study, the fixative used was 2.5% paraformaldehyde and 1.5% glutaraldehyde in 0.1 M PBS with 4% sucrose, pH 7.4. Brains from three mice were removed and postfixed in the same fixative for 1 hour followed by three washings in 0.1 M PBS with 4% sucrose. Cerebella were coronally sectioned with a Vibratome at 60 μm thickness, and alternate sections were processed for CO cytochemistry (Wong-Riley, 1979) or for further postembedding CO immunocytochemistry. Both types of sections were osmicated in 0.5% osmium tetroxide for 1 hour at RT, dehydrated in an alcoholic series, and embedded in Durcupan resin as described previously (Nie and Wong-Riley, 1995).

CO immunohistochemistry

Free-floating sections were blocked for 12 hour at 4°C in PBS-NFDM containing 1% Triton X-100 and 5% (vol/vol) normal goat serum (NGS). After rinsing in PBS, serial sections were incubated in primary antibodies diluted in PBS-NFDM with 1% Triton X-100 and 5% NGS: (1) anti-CO III at 1:2,000; (2) anti-CO Vb at 1:2,000; and (3) preimmune sera at 1:2000, for 4 hours at RT, then for 24 hours at 4°C. The sections were rinsed, then incubated with secondary antibodies (Bio-Rad blotting grade GaR-HRP) at 1:100 in PBS-NFDM with 5% NGS for 12 hours at 4°C. Sections were rinsed in 0.1 M NaPi, pH 7.0 (NH_4OH), then incubated in the same buffer with 0.5% (wt/vol) 3,3′-diaminobenzidine 4 HCL (DAB) and 0.004% (wt/vol) H_2O_2 for 5–10 minutes at RT. The DAB-incubated sections were rinsed with PBS, then mounted and coverslipped by standard procedures.

Postembedding immunocytochemistry for CO

Ultrathin sections of cerebella were cut and placed on nickel mesh grids. The following procedures, as described previously (Nie and Wong-Riley, 1995), with minor modifications were used for postembedding CO immunocytochemistry. Ultrathin sections were treated with 4% aqueous solution of sodium metaperiodate for 40 minutes and rinsed three times in distilled water. They were then placed in Tris (10 mM) phosphate (10mM) buffered isotonic saline (TPBS), pH 7.6, containing 0.1% Triton X-100 and 1% NGS for 30 minutes. Grids were then transferred to drops containing either the CO III purified IgG diluted at 1:100 or the CO Vb purified IgG at 1:100 in the same TPBS buffer. The concentrations of the two primary antibodies were determined mainly based on the findings that the numbers of gold particles reached a saturation level when the sections were incubated at a concentration of more than 6 μg/ml for each antibody. The incubation time in the primary antibodies was 6 hours at RT. Afterwards, sections were rinsed three

times in TPBS and then incubated in the secondary antibodies (goat anti-rabbit IgG conjugated to 10 nm colloidal gold, Amersham) diluted 1:15 in TPBS, pH 8.2, for 2 hours at RT. After rinses in TPBS and distilled water, the sections were stained with alcoholic uranyl acetate and lead citrate, rinsed again, air dried, and viewed under the electron microscope. To evaluate the specificity of these two antibodies, sections were processed in the same way as described above, except that the primary antibodies were preadsorbed with their corresponding subunit synthesized peptide-glutaraldehyde-KLH conjugate, or replaced with preimmune sera. In both controls, CO III or CO Vb immunoreactivity was completely abolished.

Optical density analysis

To assess the intensity of reaction product of CO histochemistry and immunohistochemistry of CO III and CO Vb, optical density measurements were made on sections of superior colliculi (SC) of monocularly enucleated mice by means of a Zeiss photometer attached to a Zeiss compound microscope. Twenty readings were taken from the retinorecipient superficial gray layer of SC of each mouse. All lighting conditions, magnifications, and reference points were kept constant.

Quantitative analysis at the EM level

Extensive quantitative EM analysis was performed on both CO histochemically treated sections and CO immunocytochemically processed sections of cerebella from three mice. We used a two dimensional method for data collection and analysis, as described previously (Wong-Riley et al., 1989a; Nie and Wong-Riley, 1995). Specifically, the areal densities of various neuronal profiles and mitochondria within them were determined from electron micrographs. All samples were treated identically to minimize technical variations. Two assumptions were made: first, the distribution and orientation of all sampled elements were random; and second, the effects of fixation and tissue processing did not vary with region or with profile size. Based on these assumptions, mitochondria in the following neuronal profiles, identified by their fine structural features, were quantitatively analyzed: (1) dendrites in the molecular layer, (2) mossy fiber terminals in the granule layer, (3) basket terminals around Purkinje cell bodies, (4) granule cell bodies, and (5) Purkinje cell bodies.

1) Mitochondria and their CO activity

High-magnification electron micrographs (x 35,000) were taken from cerebellar samples. The cross-sectional area of every detectable mitochondrion within the profiles mentioned earlier was computed by using a Calcomp 9000 digitizing pad interfaced with an advanced digital microcomputer; and the degree of CO activity for each mitochondrion was determined as previously defined: darkly reactive mitochondria (D) possessed reaction product covering more than 50% of the outer surface of the inner mitochondrial membrane and filling the intracristate space. Moderately reactive ones (M) had reaction product that filled less than 50% of the inner mitochondrial membrane. Lightly reactive ones (L) had little or no detectable reaction product (Mjaatvedt and Wong-Riley, 1988; Wong-Riley et al., 1989). The percentage of mitochondria with different degrees of CO reaction was calculated for each profile examined.

2) Immunogold quantitation

Electron micrographs of the cerebellar sections processed immunocytochemically were at a magnification of x 35,000. For each antibody (either CO III or CO Vb), a total area of about 8,000 μm^2 from three mice was measured. Areal measurements of mitochondria and non-mitochondrial cytoplasm in each profile within the sections analyzed were made as described above. The density of gold particles per unit area of mitochondria versus non-mitochondrial cytoplasm was compared to determine whether their distributions were selective. The density of immuno-gold particles over mitochondria for each antibody was measured and compared among five types of neuronal compartments, as mentioned earlier.

Statistical analysis

Parametric statistics (Student's t test and analysis of variance) were used to analyze the differences between groups. Means were reported ± standard errors. A probability of 0.05 or less was considered significant.

RESULTS

Specificity of anti-CO subunit III and Vb

All antibody titers were determined by ELISA. The antibody titers for both CO III and Vb in the sera were undetectable before the first immunization, and reached a high titer (diluted at 1:200,000 for CO III and 1:200,000 for CO Vb) against the synthetic CO subunit peptides within 2 weeks after the booster. IgGs against subunit peptides were purified from crude antisera to avoid possible cross-reaction with carrier protein and/or glutaraldehyde. ELISA results showed that affinity-purified IgGs reacted specifically only with the corresponding peptides of CO subunits either alone or linked to carrier proteins (KLH), and did not cross-react with any of the other control peptide conjugates, KLH alone, or with glutaraldehyde.

The two antibodies reacted specifically with only the corresponding CO subunits from crude mouse brain tissue, as shown by SDS immunoblot analysis (Fig. 1). No immunoreactive band was detected in the controls of either preimmune sera (Fig. 1) or antisera preadsorbed with synthetic peptides (not shown).

The antibodies also reacted specifically with CO either immunohistochemically or immunocytochemically. Strong immunostaining was seen at the light microscopic level in the mouse cerebellum when anti-CO III or anti-CO Vb were used, but not when either preimmune sera (Figs. 2–3) or IgGs preadsorbed with the corresponding peptides were used (not shown). To carry out immunocytochemical analysis quantitatively, we examined whether the ultrathin sections were incubated at a saturation level of antibodies by reacting the sections with anti-CO III or anti-CO Vb at increasing concentrations of antibodies. Figure 4 showed that the number of gold particles reached a saturation level at a concentration of more than 1:160 for each antibody. Thus, we routinely incubated ultrathin sections at a concentration of 1:100 for each antibody. With postembedding CO immunocytochemistry, the ultrastructure of the cerebellum was well preserved and thus the subcellular distribution of immunoreactivity for anti-CO subunits could be clearly visualized (Fig. 5). The immunoreactive signals for the two antibodies, indicated by gold particles, were seen mainly in the inner mitochondrial membrane rather than in the extramitochon-

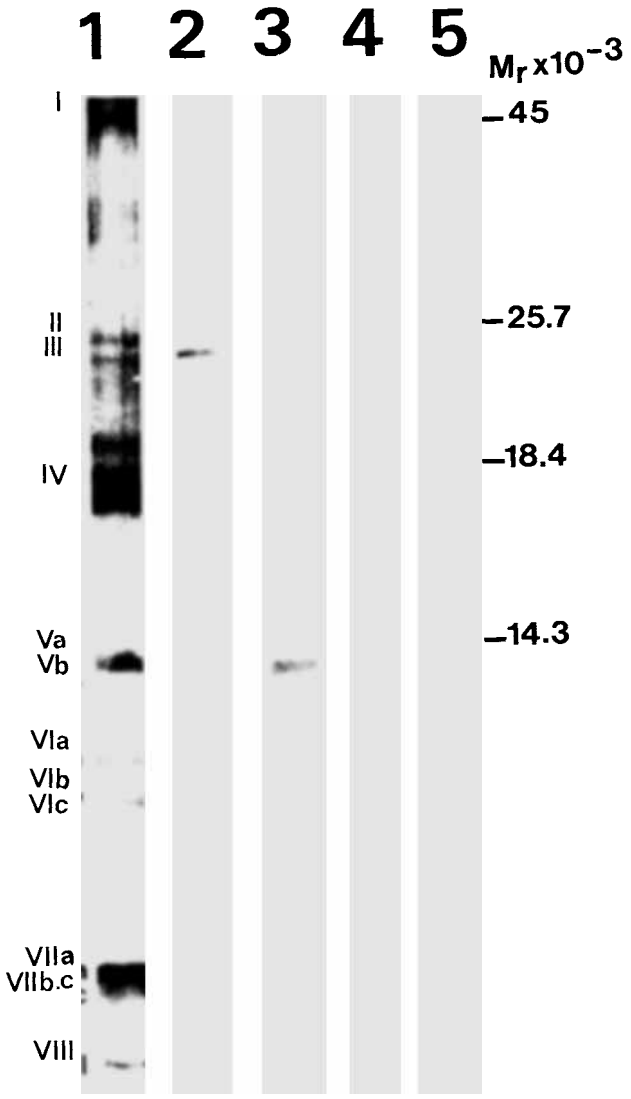

Fig. 1. Immunoblot analysis of antibody specificity for cytochrome oxidase (CO) subunit proteins. Different lanes from the same gel (18.6% T, 3.0% C) were either stained with silver to show CO subunits (**Lane 1**) or transferred to nitrocellulose and immunoblotted with anti-CO III (**Lane 2**), anti-CO Vb (**Lane 3**), or preimmune sera (**Lane 4** for CO III and **Lane 5** for CO Vb), The immunoreactive bands were visualized by Bio-Rad blotting grade GaR-HRP and diaminobenzidene (DAB). The positions of molecular weight markers are shown at the right. CO purified from bovine brains (5.0 μg) was separated into its 13 subunits by sodium dodecylsulfate-poloyacrylamide gel electrophoresis (SDS-PAGE) shown in lane 1. For lanes 2–5, crude mouse brain tissue was homogenized in 10% SDS, and an equivalent amount (50 μg/lane) was loaded in each lane. Lane 2: Anti-CO III reacted only with CO subunit III. Lane 3: Anti-CO Vb recognized only CO subunit Vb. No immunoreactive bands were seen in lanes 4 and 5 (preimmune sera).

drial cytoplasm. Quantitative analysis (Table 1) showed that the densities of gold particles over mitochondria for the two antibodies was much higher than that over non-mitochondrial regions ($P \ll 0.0001$). The control with preimmune sera showed only very low background staining, with no difference between mitochondrial and non-mitochondrial regions.

Immunohistochemistry for CO subunits and comparison with CO histochemistry

A similar pattern between immunohistochemistry for anti-CO III, anti-CO Vb, and CO histochemistry was seen in the mouse cerebellum (Fig. 3). Within this region, all three patterns showed darkly stained gray matter, and very lightly stained white matter. However, there were noticeable differences in their patterns of labeling in the same regions (Fig. 3). In the molecular layer, the dendrites of Purkinje cells were intensely stained by anti-CO III (Fig. 3a), anti-CO Vb (Fig. 3b), and CO histochemistry (Fig. 3c). However, the morphology of Purkinje cell dendritic tree was most prominent with anti-CO III and least so for anti-CO Vb. The staining of anti-CO Vb and CO histochemistry was more punctate than that of anti-CO III. In the Purkinje cell layer, Purkinje cell bodies were densely immunostained by anti-CO Vb (Fig. 3b), but only lightly or moderately reactive for anti-CO III (Fig. 3a) or CO histochemistry (Fig. 3c). The intense labeling of anti-CO III and CO histochemistry was mainly extracellular, and most likely represented reactive basket cell terminals. In contrast, intense immunoreaction product of anti-CO Vb was distributed throughout the cytoplasm of Purkinje cell bodies. In the granule cell layer, all three procedures (Fig. 3) showed a similar pattern of intensely stained patchy profiles, which were presumed to be mossy fiber terminals. However, anti-CO Vb also revealed some cell-like labeling in this layer (Fig. 3b). Thus, these results demonstrated that neuronal distribution of immunoreactivity for CO III differed from that of CO Vb, and that the immunoreactive pattern of CO III more closely matched that of CO histochemistry than of CO Vb. However, a low resolution at the light microscopic level made it virtually impossible to know whether such regional differences in their staining patterns resulted from their varying levels within the mitochondria, or from a differential areal density of mitochondria in the various compartments.

Quantitative comparisons in compartmental distribution of the two CO subunit proteins

To determine if compartmental distributions of the two subunit proteins differed, we quantitatively analyzed the density of immunogold particles for CO III and CO Vb in different neuronal profiles. Figures 5–7 show compartmental distributions of immunoreactivity for CO III and CO Vb. Mitochondria in dendrites of the molecular layer usually exhibited a dense distribution of gold particles for anti-CO III (Fig. 5a). This is consistent with our light microscopic finding that dendritic trees were intensely immunostained with this antibody. In the granule layer (Fig. 6a, Table 2), mossy fibers usually contained abundant mitochondria, most of which were intensely immunostained for anti-CO III. In contrast, substantially fewer gold particles were seen over mitochondria in granule cell bodies next to mossy fibers. In the Purkinje cell layer, mitochondria in basket terminals were more intensely labeled by anti-CO III than those in neighboring Purkinje cell bodies (Fig. 7a, Table 2), indicating that the pericellular staining of Purkinje cells found at the light level could be accounted for primarily by basket terminals. Quantitative analysis (Table 2) confirmed that the gold particle density labeled by anti-CO III over mitochondria in neuronal processes, including dendrites, mossy fibers, and basket terminals, was significantly higher

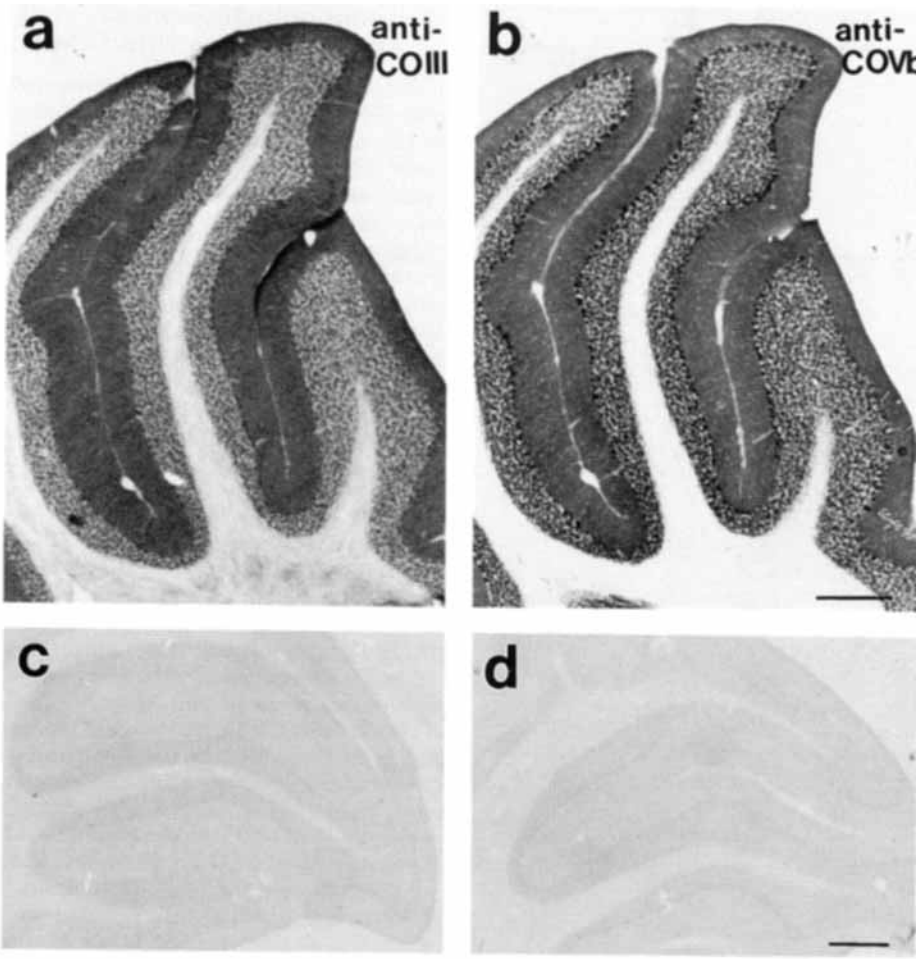

Fig. 2. Specificity of CO immunohistochemistry in the mouse cerebellum. Serial frozen sections from the same block of cerebellum were processed with immunohistochemistry for anti-CO III (**a**) and for anti-CO Vb (**b**). In a and b, the intensities of immunoreactivity are much higher in the gray matter than in the white matter. Only non-specific background staining is seen in preimmune control sections (**c, d**). Scale bars = 0.5 mm.

than that over mitochondria of either granule cell or Purkinje cell bodies ($P < 0.001$ in each case). In addition, the density of gold particles in mitochondria of dendrites was significantly higher than that in mossy fibers and basket terminals (Table 2, $P < 0.05$).

On the other hand, compartmental distribution of CO Vb immunoreactivity differed from that of CO III. There was no marked difference in gold particle distribution over dendrites and nearby profiles in the molecular layer (Fig. 5b). In the granule layer, the gold particles representing anti-CO Vb appeared evenly distributed over mitochondria of mossy fibers and granule cell bodies (Fig. 6b, Table 2). Likewise, gold particles existed uniformly over mitochondria in basket terminals and in their targets, Purkinje cell bodies (Fig. 7b, Table 2), suggesting that high immunoreactivity in both compartments may contribute to more intense staining of Purkinje cell bodies seen at the light level. Quantitative analysis showed that the density of gold particles labeled by anti-CO Vb over mitochondria in various neuronal processes, including dendrites, mossy fibers, and basket terminals, was not significantly different as compared to that in cell bodies of granule and Purkinje cells (Table 2). Thus, the distribution of CO Vb immunoreactivity was relatively homogeneous among different neuronal compartments.

Comparison of CO activity between different neuronal compartments

CO cytochemistry at the EM level (Fig. 8) showed that CO activity, as indicated by reaction product over mitochondria, was quite different between neuronal compartments, confirming our previous findings in rats (Mjaatvedt and Wong-Riley, 1988). The dendrites, basket terminals, and mossy fibers usually contained abundant mitochondria, most of which were darkly and moderately reactive for CO (Fig. 8). In contrast, somata of either Purkinje cells or granule cells consistently contained mitochondria that were primarily lightly reactive for CO (Fig. 8). Quantitative analysis showed that the proportion of darkly CO-reactive mitochondria was much higher in dendrites, mossy fibers, and basket terminals than that in cell bodies (Fig. 9, $P < 0.001$ in each case). In addition, the proportion of darkly CO-reactive mitochondria in dendrites was significantly higher than in mossy fibers and basket terminals ($P < 0.05$).

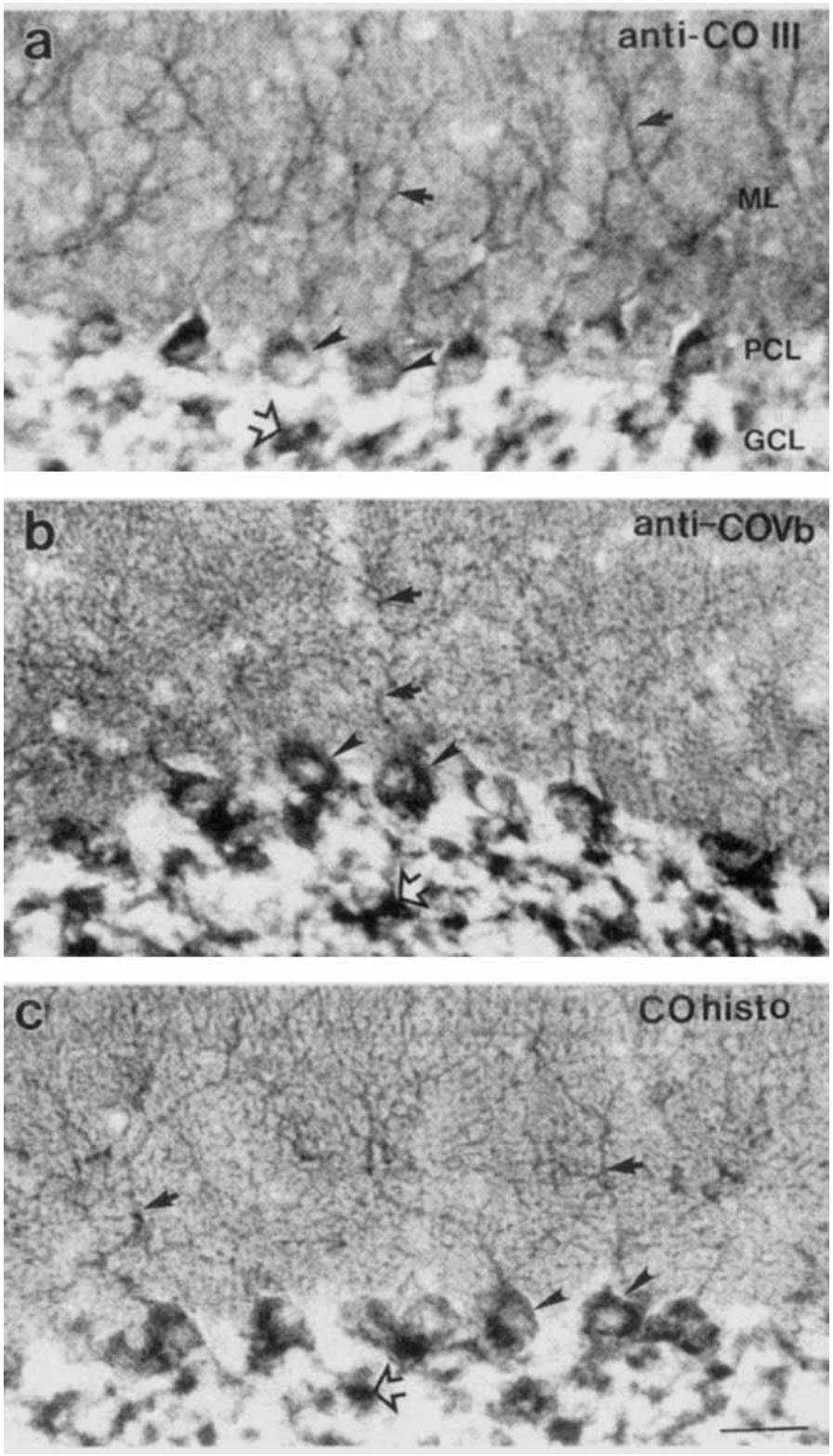

Fig. 3. Serial parasagittal frozen sections of the mouse cerebellum ere reacted for anti-CO III (**a**), anti-CO Vb (**b**), and CO histochemistry c), respectively. In the molecular layer (ML), the dendrites (solid rrows) of Purkinje cells are intensely stained by anti-CO III (a), nti-CO Vb (b), and CO histochemistry (c). However, the morphology of urkinje cell dendritic tree is most prominent with anti-CO III and ast so for anti-CO Vb. Purkinje cell bodies (arrowheads) in Purkinje ll layer (PCL) are densely immunotained by anti-CO Vb (b) and light moderately reactive for anti-CO III (a) or CO histochemistry (c). The labeling appears around (but not in) Purkinje cell bodies (arrowheads) in anti-CO III (a) and CO histochemically treated sections (c); this probably corresponds to reactive basket cell terminals. In contrast, the immunoreactive labeling with anti-CO Vb (b) is distributed throughout the cytoplasm of Purkinje cell bodies (arrowheads). In the granule cell layer (GCL), the three procedures show a similar pattern of multiple large, intensely stained patchy profiles (open arrows) which are presumed to be mossy fiber terminals (see Mjaatvedt and Wong-Riley, 1988; Liu and Wong-Riley, 1994). Scale bar = 0.03 mm.

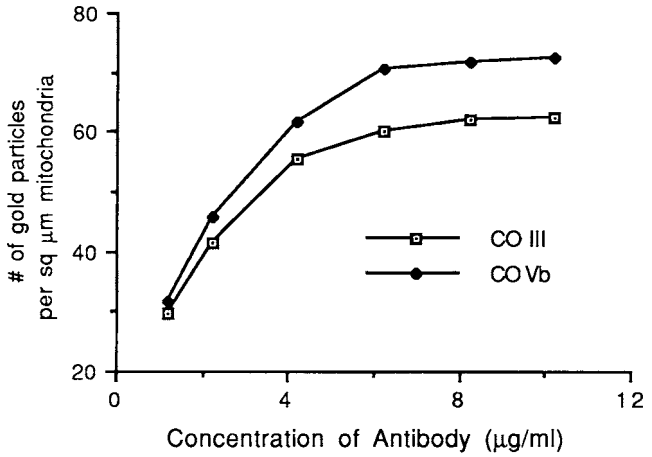

Fig. 4. Binding of immunogold particles to the mitochondria of mouse cerebellar sections. Ultrathin sections of the cerebellum were incubated in 30 µl each of increasing concentrations of affinity-purified CO III and CO Vb antibodies following 10 nm immunogold secondary antibodies (at 1:15). The particle density on the mitochondria was determined for each antibody. The average numbers of gold particles for each antibody at each concentration are shown. In both cases, binding is saturated when the antibody is at a concentration of more than 6 µg/ml (1:160). In the present study, postembedding staining was conducted using 10 µg/ml (1:100) of antibody concentrations.

The effect of enucleation on the levels of CO III, CO Vb, and CO activity

To determine whether functional activity proportionately regulates the relative amount of CO subunits III and Vb (indicated by immunohistochemistry) and the relative activity of CO (indicated by histochemistry), we quantitatively compared their changes in the deprived superior colliculus after 1 to 7 days of monocular enucleation. The murine superior colliculus consists of three cellular layers, including the superficial gray layer, intermediate gray layer, and deep gray layer. Fibers from one eye project mainly to the contralateral superior colliculus, and thus the ipsilateral side can be used for comparison. In untreated animals, the staining intensities for CO histochemistry

TABLE 1. Comparisons of Gold Particle Densities over Mitochondrial and Non-mitochondrial Area in the Cerebellum

Localization	Mean gold particles per μm^2 ± SEM	Area (μm^2)	Statistical comparisons
CO III			
Mitochondria	62.53 ± 2.42	147	$P \ll 0.0001$
Non-mitochondria	2.78 ± 0.14	6682	
CO Vb			
Mitochondria	72.47 ± 3.42	124	$P \ll 0.0001$
Non-mitochondria	3.25 ± 0.36	6154	
Preimmune			
Mitochondria	2.66 ± 0.12	188	NS
Non-mitochondria	2.92 ± 0.23	7743	

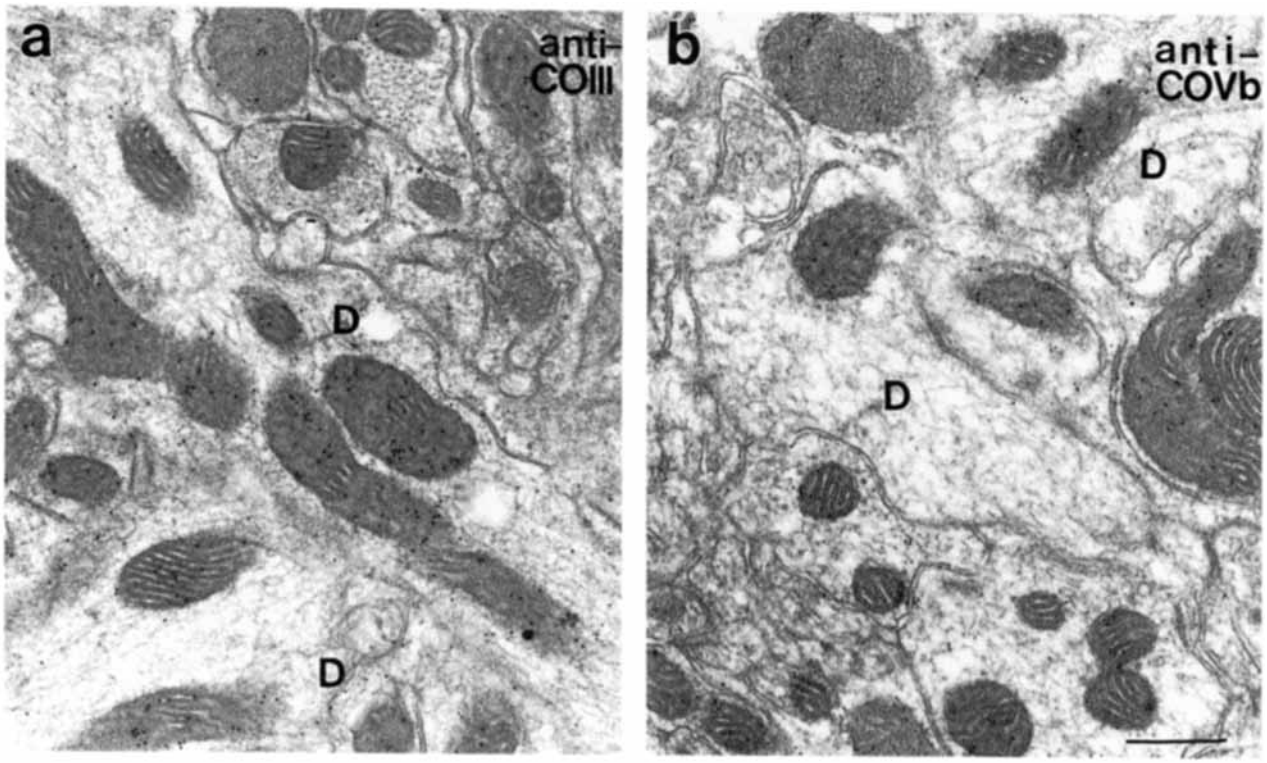

Fig. 5. Electron micrographs showing the subcellular distribution of immunoreactivity for CO III (**a**) and CO Vb (**b**). The two sections were taken from the molecular layer of a mouse cerebellum. The immunoreactivity of the two CO subunits recognized by anti-CO III (a) and anti-CO Vb (b) exist almost exclusively in mitochondria, as indicated by a highly selective localization of gold particles in mitochondria. Very few gold particles are seen in non-mitochondrial cytoplasm in both sections ($P \ll 0.0001$, see Table 1). Anti-CO III imunostaining (a) shows that the mitochondria in dendrites (D) are more intensely labeled by immunogold particles than those in other nearby profiles (see Table 2). In the section for anti-CO Vb (b), distribution of gold particles over mitochondria in dendrites (D) appears similar to that in other nearby profiles (see Table 2). Scale bar = 0.5 µm.

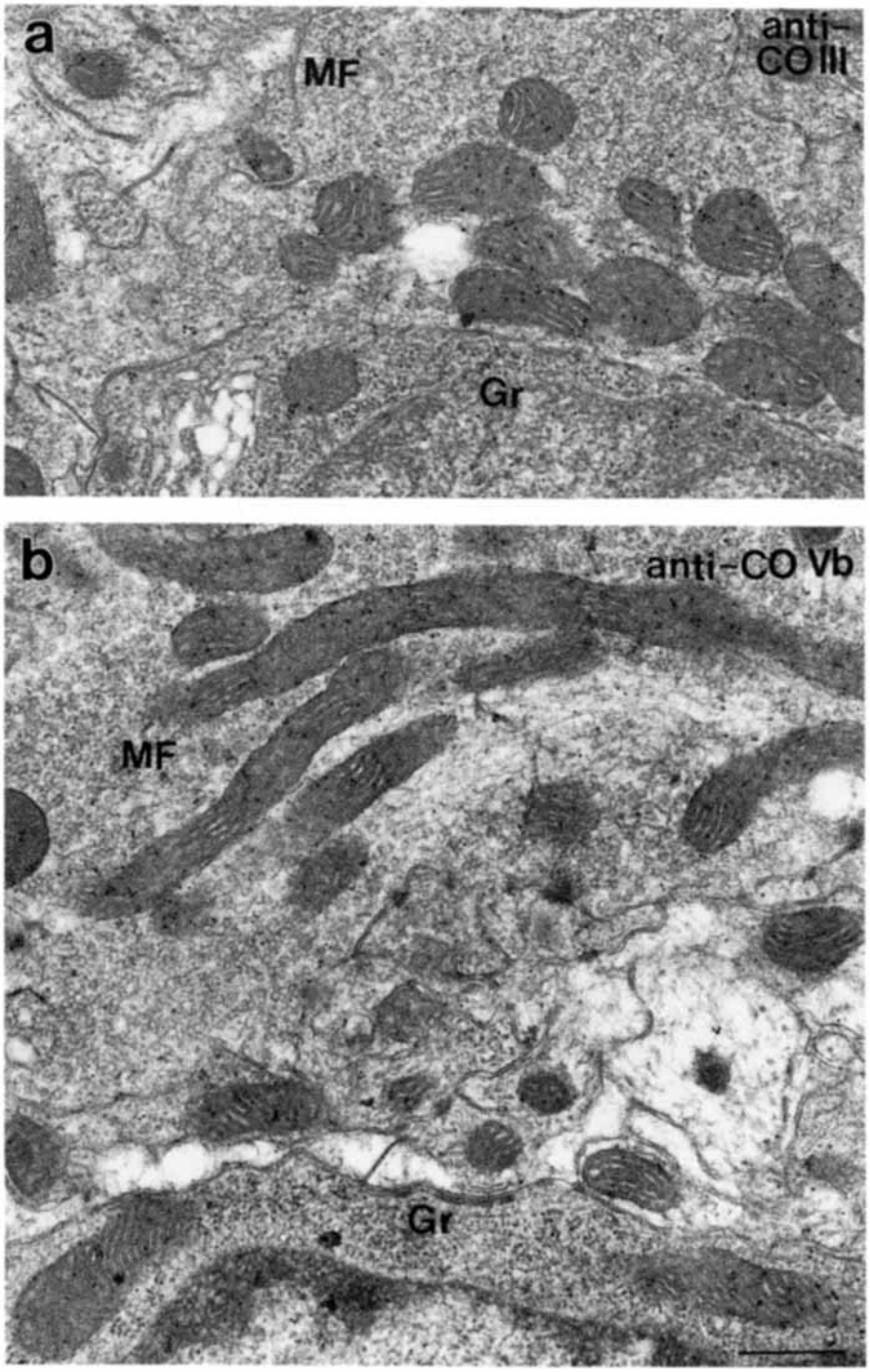

Fig. 6. Immunoreactivity of CO III (**a**) and CO Vb (**b**) in mossy fibers and granule cell bodies. The two sections were taken from the granule cell layer of the mouse cerebellum. The mossy fiber (MF) on the anti-CO III stained section (a) contains abundant densely immunoreactive mitochondria, while the mitochondria in the neighboring granule cell body (Gr) are only lightly stained ($P < 0.001$, see Table 2). In the anti-CO Vb section (b), immunoreactivity over mitochondria in mossy fiber and in granule cell body is relatively uniform (see Table 2). Scale bar = 0.5 μm.

(Fig. 10a) and CO immunohistochemistry for CO III (Fig. 10b) and for CO Vb (Fig. 10c) were comparable between the two sides of superior colliculi. One day after monocular enucleation, the intensity of labeling for the three markers in the deprived contralateral side of superior colliculus was not significantly changed as compared to the ipsilateral side (Fig. 11). However, 2 days after enucleation, the decreased staining intensities in the superficial gray layer of deprived contralateral side were visualized in sections processed with CO histochemistry (Fig. 10d) and CO III immunohistochemistry (Fig. 10e), but not with CO Vb immunohistochemistry (Fig. 10f). Optical density measurements showed that the

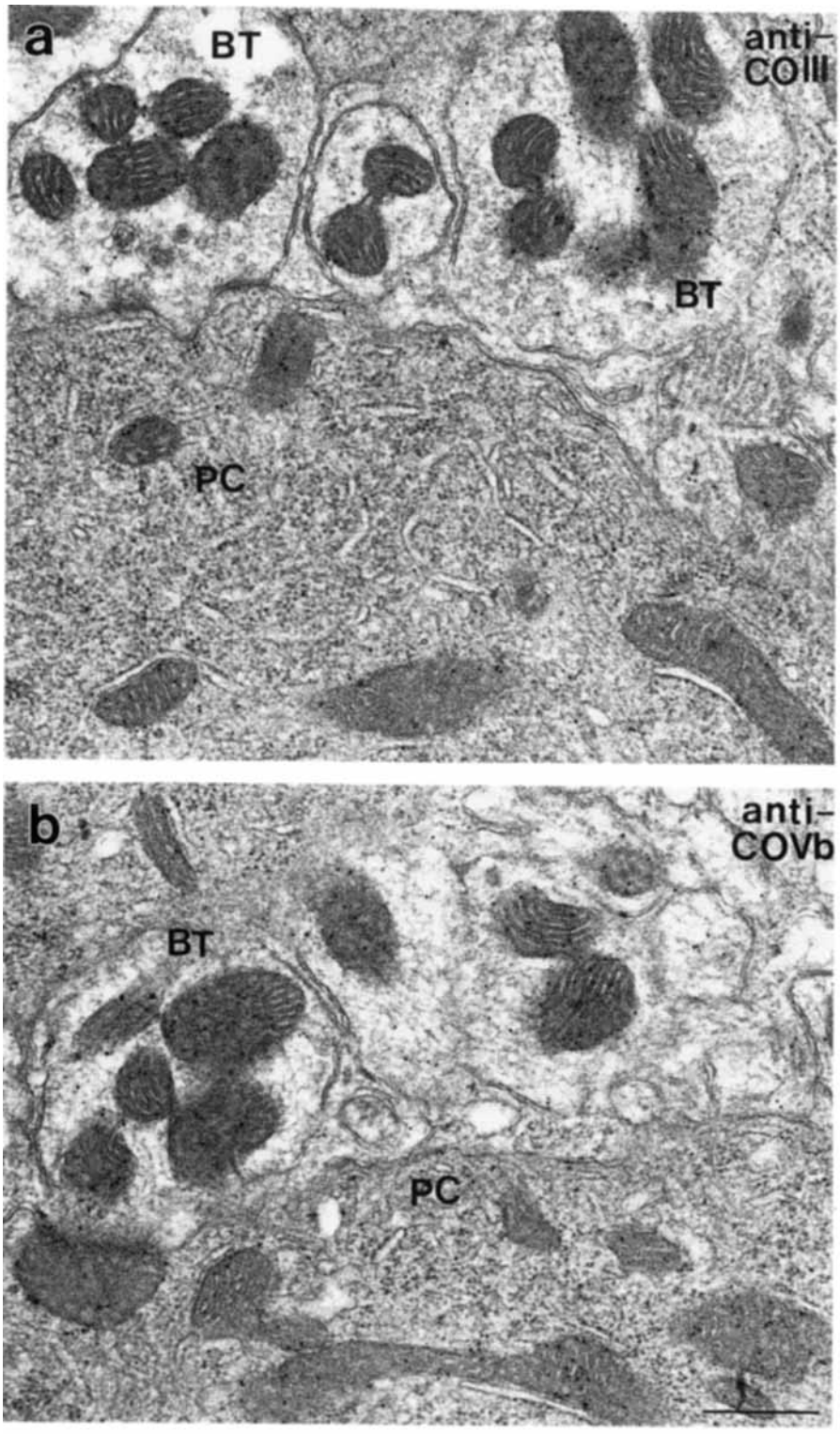

Fig. 7. Comparisons of immunoreactivity for anti-CO III (**a**) and anti-CO Vb (**b**) between Purkinje cell bodies (PC) and basket terminals (BT) of the mouse cerebellum. In anti-CO III section (a), mitochondria in basket terminals (BT) exhibit a greater immunostaining than those in Purkinje cell body (PC) ($P < 0.001$, see Table 2). In b, the gold particles representing anti-CO Vb appear evenly distributed over mitochondria of basket terminals and Purkinje cell body (see Table 2). Scale bar = 0.5 μm.

TABLE 2. Comparisons of Gold Particles over Mitochondria in Five Types of Neuronal Profiles in the Cerebellum[1]

Mitochondrial localization	Mean gold particles per μm^2 ± SEM	Measured area (μm^2)	Statistical comparisons			
CO III						
Dendrites (D)	92.34 ± 4.61	87.76	D			
Mossy Fibers (MF)	74.68 ± 3.15	112.34	*	MF		
Basket Terminals (BT)	70.92 ± 4.07	76.58	*	—	BT	
Purkinje Cells (PC)	32.40 ± 0.18	123.08	***	***	***	PC
Granule Cells	28.94 ± 0.17	38.17	***	***	***	—
CO Vb						
Dendrites	69.50 ± 3.47	91.26	D			
Mossy Fibers	73.38 ± 4.66	123.57	—	MF		
Basket Terminals	71.36 ± 5.81	69.24	—	—	BT	
Purkinje Cells	76.48 ± 6.21	111.35	—	—	—	PC
Granule Cells	75.06 ± 4.29	41.61	—	—	—	—

[1](*): $P < 0.05$, (***): $P < 0.001$, (—): NS.

intensities of both CO III immunoreactivity and CO histochemical reactivity were significantly reduced on the deprived side (Fig. 11, $P < 0.05$), while no significant change was found in CO Vb immunostained sections (Fig. 11). Four days after enucleation, the intensity of CO Vb immunostaining in the superficial gray layer of the deprived side began to exhibit a significant reduction (Figs. 10i, 11), while the levels of CO histochemical staining (Fig. 10g) and CO III immunostaining (Fig. 10h) continued to decrease (Fig. 11). From 5 to 7 days after enucleation, the staining intensities of the superficial gray layer on the deprived side progressively decreased for the three markers (Fig. 10j–l). However, the extent of their reduction was quantitatively different. At each time point examined, the percentage decrease of CO activity and CO III immunoreactivity were always significantly greater than that of CO Vb immunoreactivity (Fig. 11). By 7 days after enucleation, the intensities in CO activity, CO III, and CO Vb immunoreactivity were found to decrease by 43%, 47%, and 22%, respectively. Thus, the reduction in the levels of CO activity and CO III proteins after enucleation was earlier and to a greater extent than that of CO Vb.

DISCUSSION

The present study demonstrates that mitochondrial- and nuclear-encoded CO subunit proteins in neurons differ in their compartmental distribution, correlation with CO activity, and regulation by neuronal activity. While the distribution of mitochondrial-encoded CO III was heterogeneous and was positively correlated with that of CO activity, that of nuclear-encoded CO Vb was rather homogeneous among various neuronal compartments. Moreover, the two subunit proteins were disproportionately regulated by functional activity. Thus, the present findings suggest that the local expression and/or redistribution of CO subunit proteins from the two genomes may involve different regulatory mechanisms in neurons.

Labeling of CO subunit proteins

A direct correlation between the local amount of two different molecules in immunoreacted sections cannot be determined, because the antigen-recognizing ability for each antibody may be different. Instead, we assumed that the level of immunoreactivity of each subunit protein in different tissue profiles is positively correlated with the local amount of the protein when a saturated concentration of antibody is used. Indeed, the density of immunogold particles in an immunostained section containing a fixed antigen is reportedly proportional to the concentration of the antigen (Ottersen, 1989). It is unlikely that equivalent tissue processing would differentially affect immunoreactivity for the same antibody in different subcellular compartments (e.g., preferential mitochondrial localization of CO subunit in the present study). Thus, with identical treatment, the level of immunoreactivity for a specific CO subunit in different neuronal compartment would be determined mainly by its local amount. The antibodies for mitochondrial-encoded CO III are expected to label both the assembled and unassembled mature forms of this subunit (Kadenbach et al., 1983; Attardi and Schatz, 1988; Azzi and Muller, 1990). The antibodies against nuclear-encoded CO Vb may recognize not only its mature form, but also its precursor proteins, since its presequence might remain attached (Kaput et al., 1982; Reid et al., 1982). However, the amount of nuclear-encoded CO precursor proteins is several 100-fold less than their mature form (Liu and Wong-Riley, 1994).

Heterogeneous distribution of CO subunit proteins in neurons

One of our striking findings is that mitochondrial- and nuclear-encoded subunit proteins differ in their compartmental distribution and correlation with CO activity in neurons. At the light microscopic level, immunoreactivity for CO III in the cerebellum was more intense in neuronal processes than in cell bodies, a pattern similar to that of CO activity. On the other hand, immunoreaction product for CO Vb was uniformly distributed in cell bodies and neuronal processes of this region, consistent with previous findings (Hevner and Wong-Riley, 1989; Isashiki et al., 1991). Our quantitative EM analysis with CO immunocytochemistry confirms a homogeneous distribution of CO Vb over all neuronal compartments. However, a significantly higher level of CO III was found in mitochondria of dendrites and axon terminals than of neuronal cell bodies, in which local level of this subunit proteins closely matches that of CO activity. It is noteworthy that neuronal compartments containing high levels of CO III proteins and CO activity are also functionally more active regions (Woodward et al., 1971; Creutzfeldt, 1975). These regions include postsynaptic dendrites, which receive primarily excitatory input, and mossy fibers and basket terminals, which exhibit intense depolarizing activity (Palay and Chan-Palay 1974; Creutzfeldt, 1975). In contrast, Purkinje and granular cell bodies receive mainly inhibitory axosomatic synapses. Membrane depolarization (presynaptic or postsynaptic) would impose a greater energy demand for repolarization than would hyperpolarization (Ruscak and Whittam, 1967; Lowry, 1975; Wong-Riley, 1989, 1994). Thus, the local level of mitochondrial-encoded subunit proteins (but not of nuclear-encoded ones) is positively correlated with the local level of energy demand.

Factors attributing to the local differential levels of CO subunits

Do different mechanisms exist for regulating the local expression and/or redistribution of CO subunit proteins from the two genomes? In neurons, mitochondrial mRNAs for CO are distributed to both somata and neuronal processes (Hevner and Wong-Riley, 1991, 1993; Wong-Riley et al., 1994). The translation of mitochondrial-encoded subunits can, therefore, occur locally within individual mitochondria in different neuronal compartments. It is generally accepted that the local amount and/or stability of mRNA is a major factor for its translational efficiency. In

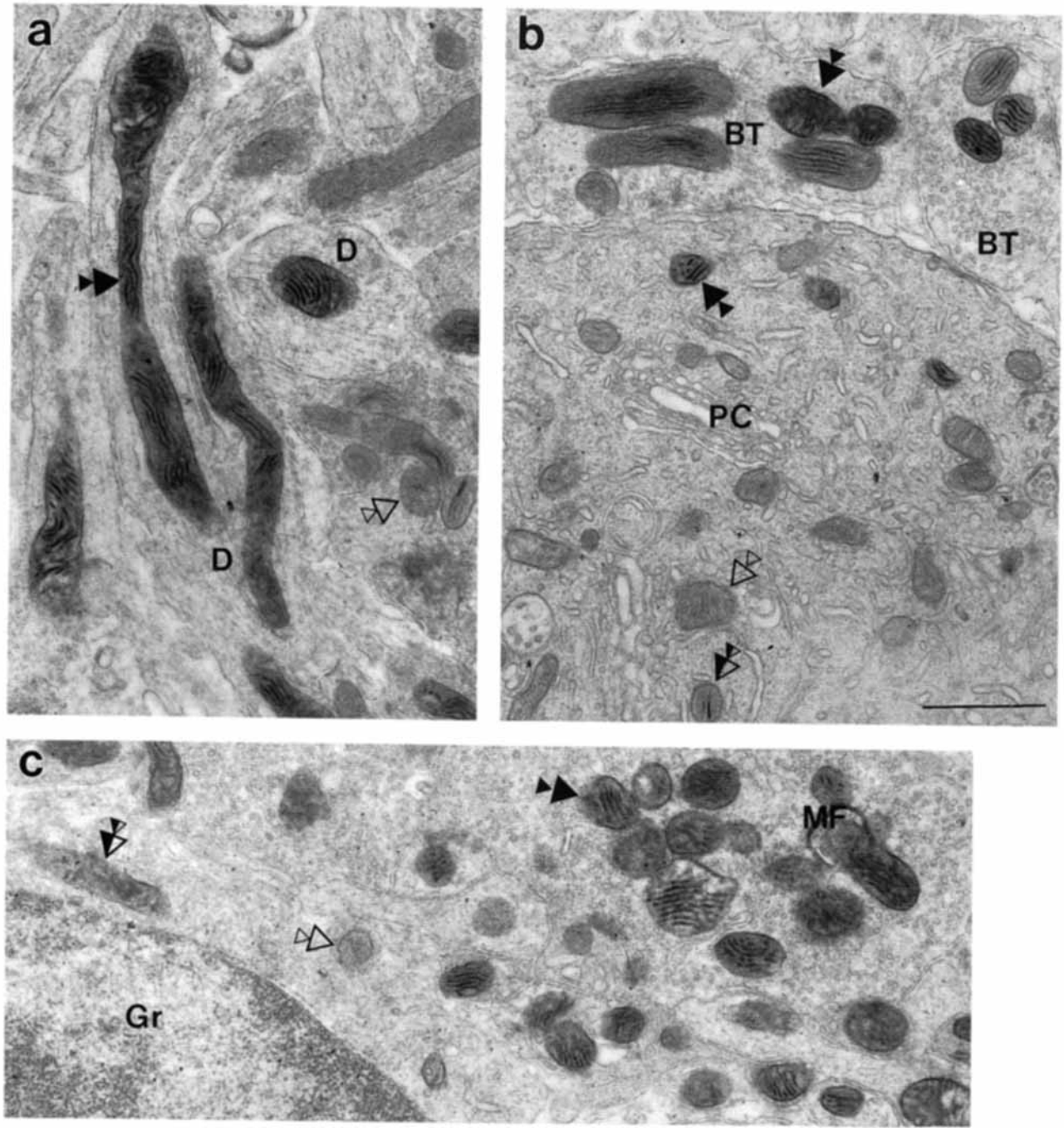

Fig. 8. Electron micrographs of mouse cerebellar sections processed for CO histochemistry. Sections were taken from the molecular layer (**a**), Purkinje cell layer (**b**), and granule cell layer (**c**). In a, the dendrites (D) contain mainly darkly CO-reactive mitochondria (double solid triangles), while many mitochondria in nearby profiles appear to be lightly CO-reactive (double open triangles). In b, basket terminals (BT) contain many mitochondria, most of which are darkly and moderately CO-reactive, but the cell body of Purkinje cell (PC) contains mitochondria that are mainly lightly reactive for CO (double open triangles). In c, most mitochondria in mossy fiber (MF) are darkly and moderately reactive for CO, while those in the granule cell body (Gr) are mainly lightly reactive, with a few moderately CO-reactive mitochondria (double half open triangles). Scale bar = 0.5 μm.

the LGN and visual cortex of normal monkeys, mitochondrial mRNAs for CO (but not for nuclear mRNAs) and CO activity exhibited a parallel distribution in each layer, which correlated with local functional activity (Hevner and Wong-Riley, 1991). For example, CO-rich puffs receive more excitatory input and contain a higher level of mitochondrial-encoded mRNA for CO than CO-poor interpuffs (Horton and Hubel, 1981; Wong-Riley and Carroll, 1984; Hevner and Wong-Riley, 1993; Nie and Wong-Riley, 1996). These results imply that an increased functional activity may locally lead to an increased expression of mitochondrial-encoded mRNA, which, in turn, may accelerate translation

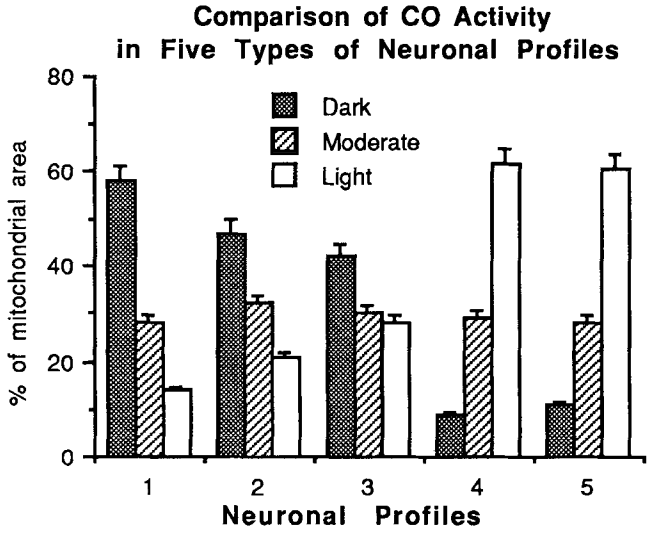

Fig. 9. Percentage distribution of mitochondria with different CO activity in five types of neuronal profiles: **1**: Dendrites from the molecular layer; **2**: mossy fibers; **3**: basket terminals; **4**: Purkinje cell bodies; and **5**: granule cell bodies. A total area of 7,400 μm^2 from three mice was measured. Mitochondria are divided into darkly, moderately, and lightly reactive according to levels of CO reactivity. Dendrites, mossy fibers, and basket terminals consistently contain a significantly higher proportion of darkly CO-reactive mitochondria than Purkinje and granule cell bodies ($P < 0.001$ for all comparisons). Dendrites also contain a higher ratio of darkly CO-reactive mitochondria than either mossy fibers or basket terminals ($P < 0.05$ in each case), while no significant difference was found between mossy fibers and basket terminals or between Purkinje and granule cell bodies.

of CO proteins. In addition, the expression of mitochondrial-encoded mRNAs among different compartments might be selectively regulated by multiple factors such as nuclear-encoded mitochondrial transcription factors (Fisher et al., 1989; Parist and Clayton, 1991). Verification of these issues needs quantitative analysis of in situ hybridization at the EM level. It is also possible that different levels of mitochondrial-encoded proteins may be caused by posttranslationally regulatory mechanisms, such as mitochondrial redistribution (Banks et al., 1969; Jeffrey et al., 1972; Morris and Hollenbeck, 1993). The greater consumption of energy in functionally active regions could lead to a local increase in ADP/ATP ratio, which can signal mitochondria to cease movement, resulting in clustering of mitochondria in regions of high ATP demand (Bereiter-Hahn and Voth, 1983). On the other hand, the nuclear-encoded CO subunits are synthesized primarily, if not only, in neuronal cell bodies, where their mRNAs are exclusively sequestered (Hevner and Wong-Riley, 1991, 1993; Wong-Riley et al., 1994). However, these nuclear-encoded subunit proteins can be posttranslationally allocated to all subcellular compartments, as indicated by their uniform distribution throughout the neuron. These results imply that CO holoenzymes can be locally assembled within mitochondria in each neuronal compartment.

The correlation between CO subunit proteins and CO activity

Does a disproportionate distribution of mitochondrial- and nuclear-encoded subunit proteins affect the assembly of CO holoenzymes in neuronal compartments? Functionally, mitochondrial-encoded subunits constitute the catalytic core of this enzyme. Nuclear-encoded subunits, on the other hand, are postulated to play a role in the regulation of CO activity and in the assembly of CO holoenzyme (Kadenbach et al., 1987; Forsburg and Guarente, 1989; Azzi and Muller, 1990; Capaldi, 1990). Depletion of either individual mitochondrial- or nuclear-encoded subunits causes a dramatic reduction in CO activity, suggesting that CO functional activity requires the existence of CO holoenzyme (Azzi and Muller, 1990; Capaldi, 1990).

The present results indicate a close correlation between mitochondrial-encoded subunit proteins and CO activity in each neuronal compartment. This implies that the local level of mitochondrial-encoded subunit proteins may represent primarily their assembled form and thus reflect the relative amount of CO holoenzymes. In contrast, the nuclear-encoded subunits are homogeneously distributed in all neuronal compartments without a close match with CO activity. They may reflect not only the assembled portions within the holoenzyme but also a significant portion that is unassembled and waiting to be processed. They form a large subunit pool for further assembly into functional enzyme (Liu and Wong-Riley, 1994). Several lines of evidence suggest that an excess amount of nuclear-encoded subunit proteins is imported into mitochondria for the synthesis of holoenzyme under normal or abnormal conditions. First, nuclear-encoded CO subunits could accumulate in the mitochondria in the absence of holoenzyme assembly in yeast, suggesting that their synthesis may depend less on the immediate demand for holoenzymes (Forsburg and Guarente, 1989). Second, free CO subunit IV (nuclear-encoded) in the mitochondria could be detected even when mitochondrial-derived subunits are depleted in human muscles with mitochondrial DNA mutation (Mita et al., 1989). Third, CO can be assembled in the absence of cytoplasmic protein synthesis for 5 hours in isolated hepatocytes, indicating that the biosynthesis of CO involves large pools of nuclear-encoded CO subunits which may preexist (Hundt et al., 1980). Fourth, the distribution of nuclear CO subunit precursors in all intraneuronal compartments provides further evidence to support the existence of nuclear subunit pool in neurons (Liu and Wong-Riley, 1994). These and our present findings support the following hypothesis: Sufficient amounts of nuclear-encoded CO subunit proteins can be intramitochondrially delivered to individual neuronal compartments for both immediate and delayed assembly of CO holoenzyme, while the local capacity for CO assembly depends mainly on the local amount of mitochondrial-encoded subunit proteins, whose distribution is closely regulated by the local energy demand. Based on this hypothesis, mitochondria in regions of higher energy demand (e.g., dendrites and active synaptic axon terminals) contain a rich supply of mitochondrial-encoded subunit proteins for local holoenzyme assembly, and thus exhibit an elevated level of CO activity. It seems unlikely that CO holoenzymes are assembled mainly in cell bodies, since both mitochondrial-encoded subunit proteins and CO activity are low in many neuronal somata. However, the mechanisms involved in each step of subunit protein processing and assembly in neurons remain elusive.

Differential regulation of CO subunit proteins and CO activity

Our above-described hypothesis is further supported by the present findings that CO activity and CO III proteins

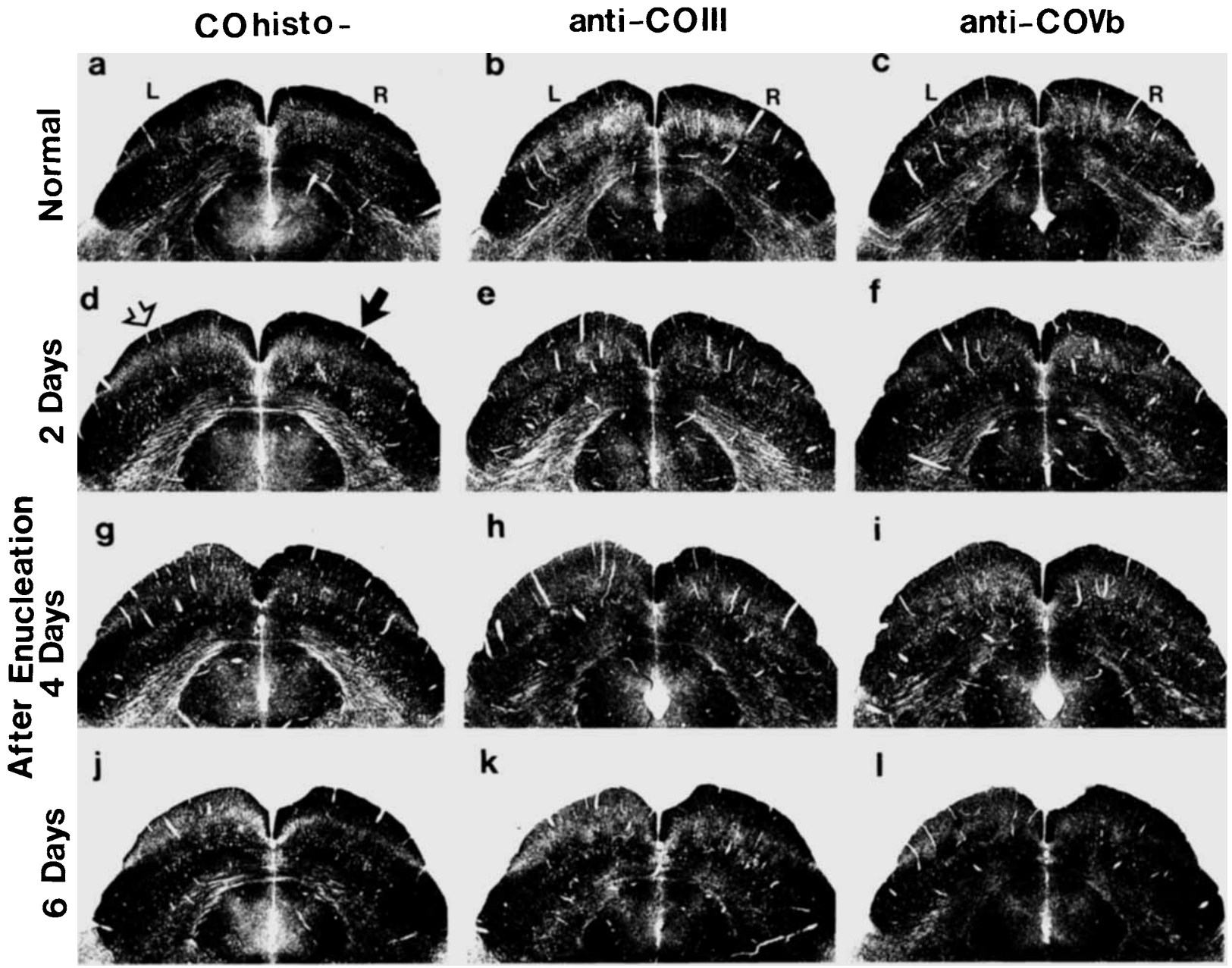
COhisto-
anti-COIII
anti-COVb
Normal
After Enucleation
2 Days
4 Days
6 Days
a
b
c
d
e
f
g
h
i
j
k
l
L
R

Figure 10

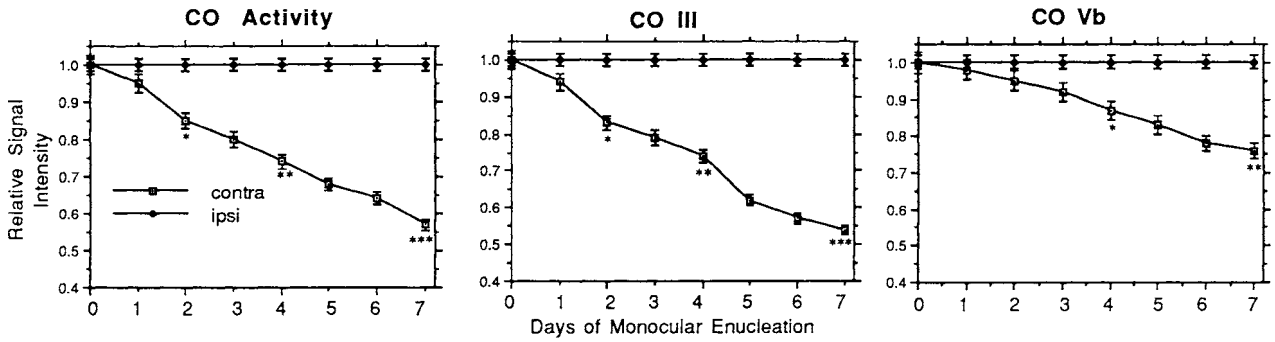

Fig. 11. Quantitative measurement of the effects of monocular enucleation on CO activity, CO III, and CO Vb immunoreactivity in the superficial gray layers of the superior colliculi (SC). Staining intensity was measured by optical densitometry in deprived and non-deprived SC in serial sections reacted for CO histochemistry, CO III, or CO Vb immunohistochemistry at each treatment period. Readings were normalized to give a mean intensity in control SC (both normal and non-deprived) of 1.00. Values plotted are mean ± SEM of 120 readings for each time point from three animals. The graphs show that the intensities of CO activity and CO III immunoreactivity in deprived SC decreased in parallel at each treatment period. This suggests that CO activity and CO III immunoreactivity fell in direct proportion to each other. The onset of the decreases in CO activity and CO III immunoreactivity was 2 days earlier than that of CO Vb, and the magnitudes of reduction in CO activity and CO III are significantly greater (up to two-fold) than that of CO Vb from 4–7 days after monocular enucleation ($P < 0.01$ at each time point). Significant differences between ipsilateral (non-deprived) and contralateral (deprived) SC are indicated by asterisks ($*P < 0.05$, $**P < 0.01$, $***P < 0.001$).

(mitochondrial-encoded), but not CO Vb proteins (nuclear-derived), are proportionately regulated by neuronal activity. Enucleation results in the removal of retinotectal terminals (Lund and Lund, 1971a, b). Although the normal level of CO in retinotectal terminals is not known, the level of CO in retinogeniculate terminals tends to be low (Kageyama and Wong-Riley, 1984). Thus, the decrement of CO levels in the superior colliculus is likely to occur primarily in postsynaptic neurons which are deprived of their presynaptic excitatory input. Parallel changes in CO activity and CO III level imply that the amount of mitochondrial-derived subunits may play a dominant role in controlling the level of CO holoenzyme and its activity during the period of adjustment. In muscle, stimulation-induced increases in CO activity were blocked by chloramphenicol-inhibition of mitochondrial protein synthesis (Williams and Harlan, 1987), suggesting that an increased CO activity may depend mainly on mitochondrial protein synthesis. Likewise, reduction of CO activity in CO-deficient muscle is always accompanied by parallel changes in mitochondrial subunit proteins, while changes in nuclear ones are much less severe and are variable (Johnson et al., 1988; Mita et al., 1989). At the transcriptional level, Williams et al. (1987) found that cytochrome b mRNA (mitochondrial) increased three-fold more than CO VIc mRNA (nuclear) after 21 days of muscle stimulation. Similarly, afferent alteration leads to changes in the level of mitochondrial-encoded mRNAs for CO I to a greater extent than that of nuclear ones (CO IV and CO VIII) in neurons (Hevner and Wong-Riley, 1993). Thus, disproportionate regulation in the expression of CO subunit proteins from the two genomes can be largely accounted for by differential changes in their mRNA levels. Taken together, the activity-dependent regulation of mRNAs and proteins for mitochondrial-encoded CO subunits is likely to play a major role in controlling the local levels of CO content and its activity in neurons, since they constitute the catalytic core of this enzyme.

However, the present study and others do not include a parallel comparison of all CO subunits at both translational and transcriptional levels. We cannot rule out whether the regulation of each individual CO subunit follows the same mechanism. For example, different nuclear-encoded subunits might be differentially regulated, since they displayed a great variety of change in their proteins (Johnson et al., 1988; Liu and Wong-Riley, 1995) and mRNAs (Williams and Harlen, 1987; William et al., 1987; Hevner and Wong-Riley, 1993). One of the ways to probe this issue further is to compare quantitatively the time course and degree of change in each subunit proteins and their mRNAs in this experimental system.

Fig. 10. Effects of monocular enucleation (1–7 days) on CO III and CO Vb proteins and CO activity in adjacent sections of mouse superior colliculi (SC). Normal superior colliculi were processed for CO histochemistry (**a**), anti-CO III (**b**), and anti-CO Vb immunohistochemistry (**c**). These sections show a symmetric staining pattern between the left (L) and right (R) sides of the superior colliculi. After monocular enucleation (right eye), the contralateral SC (left side, indicated by an open arrow) in (**d**), was deprived of afferent input, while the ipsilateral SC (right side, indicated by solid arrow) in (d) was used as a comparison. The reactive intensity for the three markers in the ipsilateral non-deprived SC was unchanged by monocular enucleation within the experimental period (7 days) as compared to normal SC. After 2 days of monocular enucleation, CO activity (d) and CO III immunoreactivity (**e**) were decreased in the contralateral SC as compared to the ipsilateral SC, but no visible change was observed in CO Vb immunoreactivity (**f**) (see Fig. 11). The intensity of CO Vb immunoreactivity began to exhibit a reduction after 4 days of monocular enucleation in the deprived SC (**i**), but the degree of change is relatively less than that of CO activity (**g**) and of CO III immunoreactivity (**h**) (see Fig. 11). Six days following the treatment, the levels of CO activity, CO III and CO Vb immunoreactivity continually fell, but decreases in CO activity (**j**) and CO III immunoreactivity (**k**) remain relatively greater than that of CO Vb immunoreactivity (**l**) (see Fig. 11). Enucleation-induced changes mainly occurred in the superficial gray layers of SC. Scale bar = 0.5 mm.

ACKNOWLEDGMENTS

Peptide synthesis was performed by the Protein/Nucleic Acid Shared Facility of the Medical College of Wisconsin, under the directorship of Dr. L. Mende-Mueller. This study was supported by NIH grants EY05439 and NS18122.

LITERATURE CITED

Attardi, G., and G. Schatz (1988) Biogenesis of mitochondria. Ann. Rev. Cell Biol. 4:289–333.

Azzi, A., and M. Muller (1990) Cytochrome c oxidase: Polypeptide composition, role of subunits, and location of active metal centers. Arch. Biochem. Biophys. *280*:242–251.

Banks, P., D. Mangnall, and D. Mayor (1969) The re-distribution of cytochrome oxidase, noradrenaline and adenosine triphosphate in adrenergic nerves constricted at two points. J. Physiol. *200*:745–762.

Basu, A., and N.G. Avadhani (1991) Structural organization of nuclear gene for subunit Vb of mouse mitochondrial cytochrome c oxidase. J. Biol. Chem. *266*:15450–15456.

Bereiter-Hahn, J., and M. Voth (1983) Metabolic control of shape and structure of mitochondria in situ. Biol. Cell *47*:309–322.

Bibb, M.J., R.A. Van Etten, C.T. Wright, M.W. Walberg, and D.A. Clayton (1981) Sequences and gene organization of mouse mitochondrial DNA. Cell *26*:167–180.

Capaldi, P.A. (1990) Structure and assembly of cytochrome c oxidase. Arch Biochem. Biophys. *280*:252–262.

Creutzfeldt, O.D. (1975) Neurophysiological correlations of different functional states of the brain. In D.H. Ingvar and N.A. Lassen (eds): Brain Work. Alfred Benzon Symposium VIII. New York: Academic Press, pp. 21–46.

DeYoe, E.A., T.C. Trusk, and M. Wong-Riley (1995) Activity correlates of cytochrome oxidase-defined compartments in granular and supragranular layers of primary visual cortex of the macaque monkey. Vis. Neurosci. *12*:629–639.

Duckrow, R.B., L.C. deManna, and M. Rosenthal (1981) Direct electrical stimulation of the cerebral cortex suggests that vascular as well as metabolic factors determine the oxidative response. Soc. Neurosci. Abstr. *7*:787.

Erecinska, M., and I.A. Silver (1989) ATP and brain function. J. Cereb. Blood Flow Metab. *9*:2–19.

Fisher, R.P., M.A. Parisi, and D.A. Clayton (1989) Flexible recognition of rapidly evolving promoter sequences by mitochondrial transcription factor 1. Genes Dev. *3*:2202–2217.

Forsburg, S.L., and L. Guarente (1989) Communication between mitochondria and the nucleus in regulation of cytochrome genes in yeast Saccharomyces cerevisiae. Annu. Rev. Cell Biol. *5*:153–180.

Grafstein, B., and D.S. Forman (1980) Intracellular transport in neurons. Physiol. Rev. *60*:1167–1283.

Harlow, E., and D. Lane (1988) Antibodies. A Laboratory Manual. New York: Cold Spring Harbor Laboratory.

Hevner, R.F., and M.T.T. Wong-Riley (1989) Brain cytochrome oxidase: purification, antibody production, and immunohistochemical/histochemical correlations in the CNS. J. Neurosci. *9*:3884–3898.

Hevner, R.F., and M.T.T. Wong-Riley (1990) Regulation of cytochrome oxidase protein levels by functional activity in the macaque monkey visual system. J. Neurosci. *10*:1331–1340.

Hevner, R.F., and M.T.T. Wong-Riley (1991) Neuronal expression of nuclear and mitochondrial genes for cytochrome oxidase (CO) subunits analyzed by in situ hybridization: Comparison with CO activity and protein. J. Neurosci. *11*:1942–1958.

Hevner, R.F., and M.T.T. Wong-Riley (1993) Mitochondrial and nuclear gene expression for cytochrome oxidase subunits are disproportionately regulated by functional activity in neurons. J. Neurosci. *13*:1805–1819.

Hundt, E., M. Trapp, and B. Kadenbach (1980) Biosynthesis of cytochrome c oxidase in isolated rat hepotocytes. FEBS Lett. *115*:95–99.

Horton, J.C., and D.H. Hubel (1981) Regular patchy distribution of cytochrome-oxidase staining in primary visual cortex of macaque monkey. Nature *292*:762–764.

Isashiki, Y., M. Nakagawa, and I. Higuchi (1991) Immunohistochemistry of the monkey retina with a monoclonal antibody against subunit V of cytochrome c oxidase. ACTA Ophthal. *69*:321–326.

Jeffrey, P.L., K.A.C. James, A.D. Kidman, A.M. Richards, and L. Austin (1972) The flow of mitochondria in chicken sciatic nerve. J. Neurobiol. *3*:199–208.

Johnson, M.A., B. Kadenbach, M. Droste, S.L. Old, and D.M. Turnbull (1988) Immunocytochemical studies of cytochrome oxidase subunits in skeletal muscle of patients with partial cytochrome oxidase deficiencies. J. Neurol. Sci. *87*:75–90.

Kadenbach, B., J. Jarausch, R. Hartmann, and P. Merle (1983) Separation of mammalian cytochrome c oxidase into 13 polypeptides by a sodium dodecyl sulfate-gel electrophoretic procedure. Anal. Biochem. *129*:517–521.

Kadenbach, B., L. Kuhn-Nentwig, and U. Buge (1987) Evolution of a regulatory enzyme: cytochrome c oxidase (complex IV). Curr. Top. Bioeneg. *15*:113–161.

Kageyama, G.H., and M. Wong-Riley (1984) The histochemical localization of cytochrome oxidase in the retina and lateral geniculate nucleus of the ferret, cat, and monkey with particular reference to retinal mosaics and ON-/OFF-center visual channels. J. Neurosci. *4*:2445–2450.

Kaput, J., S. Goltz, and G. Blobel (1982) Nucleotide sequence of the yeast nuclear gene for cytochrome c perooxidase precursor. J. Biol. Chem. *257*:15054–15058.

Krnjevic, K (1975) Coupling of neuronal metabolism and electrical activity. In D.H. Ingvar and N.A. Lassen (eds): Brain Work. The Coupling of Function, Metabolism, and Blood Flow in the Brain. New York: Academic Press, pp. 65–78.

Liu, S., and M.T.T. Wong-Riley (1994) Nuclear-encoded mitochondrial precursor protein: Intramitochondrial delivery to dendrites and axon terminals of neurons and regulation by neuronal activity. J. Neurosci. *14*:5338–5351.

Liu, S., and M.T.T. Wong-Riley (1995) Disproportionate regulation of nuclear- and mitochondrial-encoded cytochrome oxidase subunit proteins by functional activity in neurons. Neuroscience *67*:197–210.

Livingstone, M.S., and D.H. Hubel (1984) Anatomy and physiology of a color system in the primate visual cortex. J. Neurosci. *4*:309–356.

Lowry, O.H. (1975) Energy metabolism in brain and its control. In: D.H. Ingvar and N.A. Lassen (eds): Brain Work, Alfred Benzon Symposium, VIII. New York: Academic Press, pp. 48–64.

Lund, R.D., and J.S. Lund (1971a) Modifications of synaptic patterns in the superior colliculus of the rat during development and following deafferentation. Vis. Res. Suppl. *3*:281–198.

Lund, R.D., and J.S. Lund (1971b) Synaptic adjustment after deafferentation of the superior colliculus of the rat. Science *171*:804–807.

Mata, M., D.J. Fink, H. Gainer, C.B. Smith, L. Davidsen, H. Savaki, W.J. Schwartz, and L. Sokoloff (1980) Activity-dependent energy metabolism in rat posterior pituitary primarily reflects sodium pump activity. J. Neurochem. *34*:213–215.

Mita, S., B. Schmidt, E.A. Schon, S. DiMauro, and E. Bonilla (1989) Detection of "deleted" mitochondrial genomes in cytochrome c oxidase-deficient muscle fibers of a patient with Kearns-Sayre syndrome. Proc. Natl. Acad. Sci. USA *86*:9509–9513.

Mjaatvedt, A.E., and M.T.T. Wong-Riley (1988) The relationship between synaptogenesis and cytochrome oxidase activity in Purkinje cells of the developing rat cerebellum. J. Comp. Neurol. *277*:155–182.

Morris, R.L., and P.J. Hollenbeck (1993) The regulation of bi-directional mitochondrial transport is coordinated with axonal outgrowth. J. Cell Sci. *104*:917–927.

Nie, F., and M.T.T. Wong-Riley (1995) Double labeling of GABA and cytochrome oxidase in the macaque visual cortex: Quantitative EM analysis. J. Comp. Neurol. *356*:115–131.

Nie, F., and M.T.T. Wong-Riley (1996) Differential glutamatergic innervation in cytochrome oxidase-rich puffs and -poor interpuffs in macaque striate cortex: Quantitative EM analysis of neurons and neuropil. J Comp. Neurol. *369*:571–590.

Ottersen, O.P. (1989) Postembedding immunogold labeling of fixed glutamate: an electron microscopic analysis of the relationship between gold particle density and antigen concentration. J. Chem. Neuroanat. *2*:57–67.

Palay, S.L., and V. Chan-Palay (1974) Cerebellar Cortex. New York: Springer.

Poyton, R.O., C.E. Trueblood, R.M. Wright, and L. E. Farrell (1988) Expression and function of cytochrome c oxidase subunit isologues. In M. Brunori and B. Chance (eds): Cytochrome Oxidase: Structure, Function, and Physiopathology. New York: Academy of Sciences, pp. 289–307.

Reid, G.A., T. Yonetani, and G. Schatz (1982) Import of proteins into mitochondria: Import and maturation of the mitochondrial intermembrane space enzymes cytochrome b2 and cytochrome c peroxidase in intact yeast cells. J. Biol. Chem. *257*:13068–13074.

Ruscak, M., and R. Whittam (1967) The metabolic response of brain slices to agents affecting the sodium pump. J. Physiol. *19*:595–610.

Towbin, H., T. Staehelin, and J. Gordon (1979) Electrophoretic transfer of proteins from polyacrylamide gels to nitrocellulose sheets: Procedure and some applications. Proc. Natl. Acad. Sci. USA *76*:4350–4354.

Wikstrom, M., K. Krab, and M. Saraste (1981) Cytochrome Oxidase: A Synthesis. New York: Academic Press.

Williams, R.S., and W. Harlan (1987) Effects of inhibition of mitochondrial protein synthesis in skeletal muscle. Am. J. Physiol. *253*:C866–871.

Williams, R.S., M. Garcia-Moll, J. Mellor, S. Salmons, and W. Harlan (1987) Adaption of skeletal muscle to increased contractile activity: expression of nuclear genes encoding mitochondrial proteins. J. Biol. Chem. *262*: 2764–2767.

Wong-Riley, M.T.T. (1979) Changes in the visual system of monocularly sutured or enucleated cats demonstrable with cytochrome oxidase histochemistry. Brain Res. *171*:11–28.

Wong-Riley, M.T.T. (1989) Cytochrome oxidase: An endogenous metabolic marker for neuronal activity. Trends Neurosci. *12*:94–101.

Wong-Riley, M.T.T. (1994) Dynamic metabolic organization and plasticity revealed by cytochrome oxidase. In A. Peters and K.S. Rockland (eds): Cerebral Cortex. Vol. 10. Primate Visual Cortex. New York: Plenum Press, pp. 141–200.

Wong-Riley, M., and E.W. Carroll (1984) The effect of impulse blockage on cytochrome oxidase activity in the monkey visual system. Nature *307*:262–264.

Wong-Riley, M.T.T., S.C. Tripathi, T.C. Trusk, and D.A. Hoppe (1989) Effect of retinal impulse blockage on cytochrome oxidase-rich zones in the macaque striate cortex. I. Quantitative EM analysis of neurons. Vis. Neurosci. *2*:483–497.

Wong-Riley, M.T.T., M. Mullen, M. Neitz, and Z. Huang (1994) Cytochrome oxidase subunit genes: Isolation, subcloning, in situ hybridization of transcripts, and regulation by neuronal activity. Neurosci. Abstr. *20*:51.

Woodward, D.J., B.J. Hoffer, G.R. Siggins, and F.E. Bloom (1971) The ontogenetic development of synaptic junctions, synaptic activation and responsiveness to neurotransmitter substances in rat cerebellar Purkinje cells. Brain Res. *34*:73–79.